Synthesis and characterization and comparative studies of Ni, Cu, Mn, Co, Fe doped ZnO

Jyostna Chauhan[*1], Varsha R Mehto[2] and Shikha gangwar[1]

[1]HOD SONT, Rajiv Ganhi Techanical University, Bhopal (M.P.)
[2]Rajiv Ganhi Techanical University, Bhopal (M.P.)
***Corresponding author: jyotsnachauhan2006@gmail.com

Abstract: ZnO is a typical II-IV semiconductor exhibiting excellent electrical, optical and chemical properties with band gap energy (E_G) of 3.1-3.4 eV. It has a very large excitation binding energy of 60 meV at room temperature, which is very close to that of TiO_2. It is considered to be more suitable for photocatalysis applications due to its high photosensitivity, and chemical stability.

1. Introduction

1.1 morphology as ZnO

Recently, special interest has been shown in its morphology as ZnO can form various nanostructures suitable for a variety of applications in UV-shielding materials, gas sensors, biosensors, semiconductors, piezoelectric devices, field emissions displays, photocatalytic degradations of pollutants and antimicrobial treatments [1-3].

Several physical parameters such as surface area, particle size, surface charge, and zeta potential of a material are very important for its applications and functions. These physical factors of nanoparticles govern the stability, persistence and chemical or biological activities inside the living cells. ZnO nanoparticles are non-toxic, bio-safe and biocompatible and have been found in many biological applications in daily life. ZnO has been used extensively in the formulation of many personal care products such as calamine lotion, sunscreen lotion etc [4].

The novel electrical, mechanical, chemical and optical properties are introduced, which are largely believed to be the result of surface and quantum confinement effects [5].

1.2   Crystal Structure of ZnO

ZnO is a wide bandgap (3.4eV) II-IV compound semiconductor having stable wurtzite (B4 type) structure with lattice spacing a = 0.325 nm and c = 0.521 nm at ambient pressure and temperature conditions. This is a hexagonal lattice, belonging to the space group P6₃mc. Its Pearson symbol is hP4 [58]. It can also be characterized by two interconnecting sub-lattices of Zn^{2+} and O^{2-}, such that Zn ion is surrounded by tetrahedral of O ions, and vice versa. This tetrahedral coordination in ZnO form a non-central symmetrical structure with polar symmetry along the hexagonal axis which induces the characteristic piezoelectricity and spontaneous polarization, and plays a key factor in crystal growth, etching and defect generation of ZnO [7]. In addition to wurtzite phase, ZnO also crystallizes in cubic zincblende. Zincblende ZnO is stable only by growth on cubic structures.

Study of transition metal doping on optical and structural properties in ZnO nanoparticles.
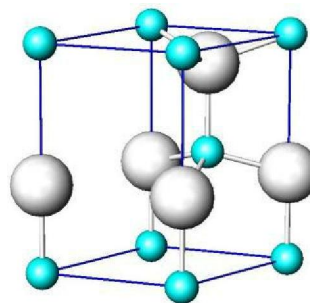

Fig. 1.2: The wurtzite structure model of ZnO. The small circles represent Zn^{2+} ions while the larger ones represent O^{2-} ions [28].

1.3 Properties of ZnO

1.3.1. Physical properties

When the dimension of bulk material is downsized to nanoscale, their physical properties undergo changes known as the "quantum size effects". For example- quantum confinement increases the bandgap energy of quasi-one-dimensional (Q1D) ZnO, which has been confirmed by photoluminescence [8]. Bandgap of ZnO nanoparticles also demonstrate such size dependence [9].

X-ray absorption spectroscopy and scanning photoelectron microscopy reveal the enhancement of surface states with the downsizing of nanorods [10]. Table 1.1 shows a compilation of basic physical parameters for ZnO [10].

Study of transition metal doping on optical and structural properties in ZnO nanoparticles.

Table 1.1: Physical parameters of wurtzite ZnO

Properties	
Lattice constants (T=300K) a0 b$_0$	0.32469 0.52069
Density	5.606 g/cm^3
Melting point	2248K
Relative permittivity	8.66
Band gap	3.1-3.4 electron volts, direct
Intrinsic carrier concentration	<10^6
Exciton binding energy	60 meV
Electron effective mass	0.24
Electron mobility (T=300K)	200 cm^2/Vs
Hole effective mass	0.59
Hole mobility (T=300K)	5-50 cm^2/Vs

1.3.2. Mechanical Properties

Based on a electric field induced resonant excitation, Bai et al characterized the bending modulus of ZnO nanobelts using TEM [11]. In this method, a special TEM sample holder was made to apply an oscillating electric field between a ZnO nanobelt and a fixed electrode. This electric field drove the vibration of the nanobelt, and resonant oscillation was achieved by tuning the driving frequency.

Following the classical elasticity theory, binding modulus wasalculated. ZnO nanobelt demonstrates to be a promising material as nanosensor and nanocantilever. The small size of ZnO nanobelt renders improved sensitivity compared with conventional cantilever fabricated by microtechnology. Hughes et al reported manipulation of ZnO nanobelt to desired length and position. Thus ZnO nanobelt can be used as an AFM cantilever with high sensitivity [6].

1.3.3. Piezoelectric Effect and Polar Surfaces

The origin of piezoelectricity in ZnO lies in its crystal structure, in which the oxygen atoms and zinc atoms are tetrahedrally bonded. In such a non-centrosymmetric structure, the center of positive and negative charges can be displaced due to external pressure induced lattice distortion (fig 1.3(a)).
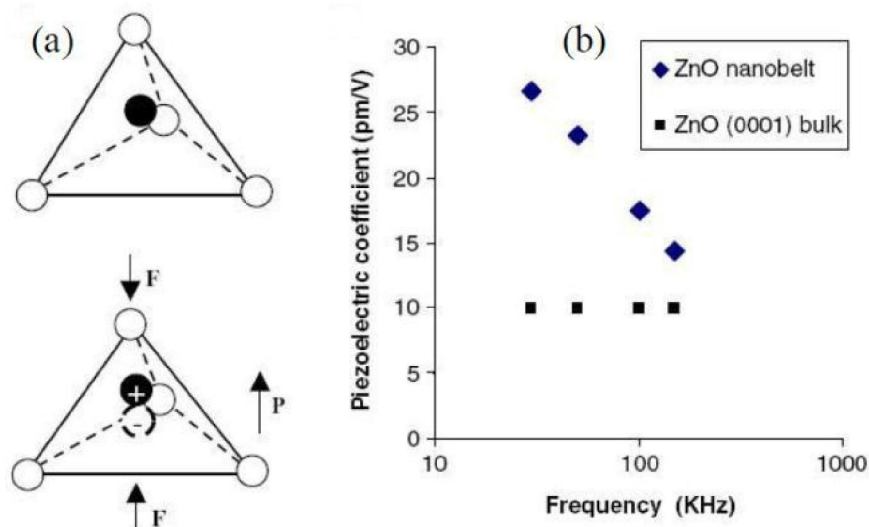

Fig 1.3:(a) Schematic showing the piezoelectric effect in tetrahedrally coordinated cation-anion unit. (b) Measured piezoelectric coefficient for ZnO nanobelt and its comparison with that of bulk. Reprint from [29], Z.L. Wang et al., Adv. Funct, Mater: 14, 943 (2004)

This displacement results in local dipole moments, thus a macroscopic dipole moment appears over the whole crystal. Among the tetrahedrally bonded semiconductors, ZnO has the highest piezoelectric tensor which provides a large electromechanical coupling [30]. The piezoelectric property of ZnO nanostructures was also investigated for their potential applications in nano-electromechanical systems. The piezoelectric coefficient of ZnO nanoparticles was measured by AFM with conductive tips [31]. The effective piezocoefficient, thus measured, is observed to be

frequency dependent and much larger than that of the bulk (0001) surface (fig 1.3 (b)). ZnO thin films have high piezoelectric coefficient values of 7-8.5 pC/N. The non-centrosymmetric ZnO crystal also results in spontaneous polarization and polar face dominated nanostructures. In ZnO crystal, the oxygen atoms and zinc atoms are tetrahedrally bonded. These tetrahedrons stack along [0001] direction. Due to spontaneous polarization, the position of positive charge is displaced from that of negative charge and the direction of displacement is also [0001]. The net result of this spontaneous polarization is a charged (0001) ZnO surface. In order to achieve minimum energy, the charged (0001) surface results in unique nano-ring and nano-coil structure.

1.3.4. Electrical Properties

Electrical transport measurements has been performed on individual ZnO nanowires and nanorods. [12]. A single ZnO nanowire was configured as field effect transistor (FET) following several procedures [13].

The CVD grown ZnO nanostructures are single crystalline, rendering them superior electrical.

property than polycrystalline thin film. For example- an electron field effect mobility of 7 cm^2/Vs is regarded quite high for ZnO thin film transistors [13]. However, single crystalline ZnO nanowires show mobility as high as 80 cm^2/Vs [12]. Park et al had reported an electron mobility of 1000 cm^2/Vs after coating the nanowires with polyimide to reduce the electron scattering and trapping at surface [14]. These results indicate that the ZnO nanostructure based devices can achieve a faster operation speed than their thin film counterpart.

In addition to electrical transport studies, electric field emission from vertically-aligned ZnO nanowire/nanorod has also been extensively researched. Field emission from vertically aligned ZnO nanoneedles and nanowires have been investigated by many groups. Tseng et al grew needle-like ZnO nanowires on Ga-doped ZnO film at 550^{0}C [16]. The as-grown nanowires showed well-aligned vertical structure. The nanowires were subject to field emission measurement, the turn-on field was found to be ~18 V/μm at a current density of 0.01μA/cm^2 and the emission current could reach 0.1 mA/cm^2 at 24 V/μm. Le et al reported better results for ZnO nanowire synthesized at low temperature [15]. A turn-on field of 6 V/μm at a current density of 0.1μA/cm^2 was obtained, and the emission current reached 1 mA/cm^2 at 11 V/μm, which could provide sufficient brightness as flat panel display. Also in the electron emission from ZnO nano-tetrapod [17, 18], a low turn-on field of 1.6 V/μm at current density of 1μA/cm^2 was reported. This is because of high aspect ratio of tetrapod structure than that of nanowires.

1.3.5. Optical Properties

Intrinsic optical properties of ZnO nanostructures are being intensively studied for implementing photonic devices. Photoluminescence (PL) spectra of ZnO nanostructures have been extensively reported [19]. Excitonic emissions have been observed from the PL spectra of ZnO nanorods [20]. It is shown that quantum size confinement can significantly enhance the exciton binding energy.

[21]. Strong emission peak at 380 nm due to band-to-band transition and green-yellow emission band related to oxygen vacancy are observed. These results are consistent with those of bulk ZnO. The green emission intensity increases with decreasing nanowires diameter. This observation is attributed to the larger surface-to-volume ratio to thinner nanowires favouring a higher level of defects and surface recombination [19, 22]. Red luminescence is also observed due to doubly ionized oxygen vacancies [23].

In ZnO nanobelts, the quantum confinement effect causes a blue shift in the near UV emission peak.

[8].PL spectra show that ZnO nanowire is a promising material for UV emission, while its UV lasing property is of more significance and interest. Due to its near-cylindrical geometry and large refractive index (~2.0) ZnO nanowire/nanorod is a natural candidate for optical waveguide. The well-facetted nanowires also form promising optical resonance cavities which greatly facilitate highly directional lasing at room temperature in well aligned ZnO nanowires [11,20]. Huang et al and Liu et al reported room temperature UV lasing from ordered ZnO nanowires array [19, 27].

1.4 Doping in ZnO

Doping is a widely used method for modification of nanoparticles esp. ZnO to enhance their electrical, optical and biological properties. Although apart from external doping, ZnO is natively doped due to oxygen vacancies or zinc interstitials. This kind of doping in ZnO is n-type. ZnO nanostructures are widely doped with transition metals viz, Mn, Fe, Co, Ni etc. Work performed in the area of transition metal doping of ZnO single crystals and thin film indicates that ZnO nanorods doped with Mn, Cr, Co formed using hydrothermal sythesis have morphologies different from that of undoped ZnO [7]. Mn is a paramagnetic element, Cu is diamagnetic while Fe, Co, Ni are ferromagnetic elements. Doping of these metal ions in ZnO give rise to a new class of materials called Dilute Magnetic Semiconductors (DMS). These materials i.e. DMS show room temperature ferromagnetism (RTFM) and are emerging as a new trend in device fabrication. Doping ZnO with a metal/metal oxide changes the band gap, photocatalytic activity and

morphology and optical properties of the materials leading to its applications in wide areas.

Due to the native defects such as oxygen vacancies and zinc interstitials, ZnO nanowires are reported to show n-type semiconductor behaviour. Since ZnO is natively n-type doped, it is quite difficult to do p-type doping in it. Several p-type doping efforts have been reported, with a Ga and N codoping method, low resistivity (0.5 Ω-cm) p-type ZnO thin film was obtained [24].

Look et al reported N-doped p-type ZnO obtained by molecular beam epitaxy with a hole mobility of 2 cm^2/Vs [25]. Kim et al reported P-doped p-type ZnO with a thermal activation process [26]. Successful p-type doping for ZnO nanostructures will greatly enhance their future applications in nanoscale electronics and optoelectronics. P-type and n-type ZnO nanowires can serve as p-n junction diodes and light emitting diodes (LEDs). And field effect transistors (FETs) fabricated from them can constitute complimentary logic circuits.

In recent years, scientists have made rapid and significant advances in the field of materials research, especially in semiconductor physics. In the last two decades, research on synthesis and characterization of inorganic semiconducting nanostructures has achieved impressive progress. Semiconductor Nanocrystals, whose electronic and optical properties are tunable, have aroused considerable interest as technologically important materials. Particularly nanoparticles formed by colloidal process have attracted attention in various disciplines, because of the capability of tailoring their physical properties simply through controlling of their size and shape. II-VI group inorganic nanoparticles such as ZnO, SnO2, TiO2, CdS, CdSe, ZnSe, and ZnTe are well-known and have been intensively studied because of their diverse luminescence, magnetic, and electric properties. Several eminent research groups were studied and analyzed that metal-modified oxide semiconductor material have the potential to act and used as catalysts, sensors, substrates for surface-enhance Raman scattering and colloidal entities with unique optical properties [22,23]. Up to now, several routes of synthesis reported by various research group at national and international level for the synthesis of ZnO [24]. Many researchers were synthesized the ZnO and characterized it. P. Kumbhakar et al [25] was shows in their work that they prepared ZnO nano particle of the average size of 1.9 nm by chemical method with PVP as capping agent and double distilled water as solvent. The density of surface states in the Nanocrystals would increase with a decrease in the size of crystallites of the prepared Nanocrystals, due to the increased surface-to-volume ratio having smaller crystallites. Effect of Cu2+ ions doping on the

photoluminescence (PL) and magnetic behavior of ZnO based host material nanoparticles was reported by. D. Sahare and V. Kumar [26] in their work. Some are trying to dope transition metals with different concentration in ZnO and analysis their optical and magnetic properties. P. K. Labhane et al [27] synthesized cu doped ZnO nanoparticles at different concentration of Cu (1%, 2% and 3%) and study about their optical and magnetic properties they reported grain size of the sample was in the range of 23-29nm.

P. M. Aneesh et al [28], M. Mazhdi [29] and Surbhi Siva Kumar et al [24] synthesized ZnO with Different methods and shows result that how reaction time, reaction temperature, calcinations temperature, concentration of the precursors affect grain size, optical and structural properties of the sample.

Experimental Part

3.1   Types   of   Conventional   Synthesis Techniques

Various routes have been developed for the preparation of different forms of ZnO nanoparticles to investigate its properties and further improvements. The different synthesis methods with different parameters and stringent growth conditions like temperature, pressure, hydrolysis ratio, and precursors have been adopted to achieve different forms of ZnO nanoparticles such as nonospheres, nanocombs, nanorings, nanoloops, nanowires, nanotubes etc [1-3]. These include MO-CVD, thermal vapour evaporation, hydrothermal synthesis, and oxidation of metallic Zn powder without metal [1,3]. These methods are broadly classified into two main routes of NPs synthesis;

1. Vapour phase synthesis.
2. Solution phase synthesis.

3.1.1   Vapour or gas phase synthesis of ZnO

In this route of synthesis of ZnO nanoparticles, the process is generally carried out in an inert gaseous environment in closed chambers at high temperatures from 500 degree C to 1500 degree C. Some of the commonly used gas phase methods are physical vapour deposition, CVD, MOCVD, thermal oxidation of pure Zn and condensation, microwave assisted thermal decomposition [5]. Different sources such as evaporation, sputtering and laser are used to evaporate materials from the surface of solids into clusters, which are then condensed, transported and collected on a substrate to form nanoparticles. By vapour phase route, high quality crystalline thin film, 2D nanostructures like nanowires, nanorods etc can be formed.

3.1.2   Solution phase synthesis of ZnO

Solution phase synthesis is also called hydrothermal growth process. In this route, the synthesis is carried out in aqueous solutions at relatively low temperatures. Examples of solution

based techniques are: sol-gel method, spin coating, spray pyrolysis, electrodeposition process of self-assembly of nanopores, chemical bath deposition etc. Solution based synthesis processes are simple and cost effective and large range of materials can be synthesized by these methods.

3.2 Implemented Synthesis Technique
3.2.1 Co Precipitation Method

In co-ppt method, the desired components are precipitated from the solution using a precipitating agent generally NaOH, etc. In co-ppt, normally soluble compounds are precipitated. Co precipitation is used for simultaneous precipitation of more than one component.

In general, the metal hydroxides are precipitated from their precursor salt solution because of their low solubility. The precipitation of hydroxides can be formed either by starting from an alkaline solution which is acidified or from acidic solution by raising the Ph.

Washing and filtering

Washing can be done by decantation. This method is time consuming. In this method the precipitate or gel is added to a large volume of distilled water and the suspension is thoroughly stirred. Then, the suspension is allowed to settle. The foreign undesirable ions are desorbed from particles as they settle down slowly at the bottom. When a clear interface is visible, the water is removed by decantation and the process is repeated. The number of washings required is determined by checking the impurity level of the decanted water. After washing, the precipitate or gel is filtered. The process can be reversed. That is the filtration is done first and the precipitate or gel is washed with distilled water in the subsequent step. This method takes less time. Impurity level in the wash water is checked to determine the required number of washings.

Drying

Drying is described as the elimination of water or solvent from the pores of the precipitate or gel. It can be done in two ways:

        Solvent evaporation
        Super critical drying

Calcinations or sintering

After the removal of pore liquid, further heat treatment is necessary to convert the precipitate or dry gel to catalytically useful form. After drying, the next step of heat treatment is known as calcination. Often the heating is done in the presence of flowing air or oxygen to burn any residual organics or to oxidize the sample. Multiple changes occur during this process including:

1. Active phase generation: The hydroxide form is converted to oxide form.

2 Stabilization of mechanical properties: The catalysts sample is subjected to a more severe heating treatment than that is likely to encounter in a reactor to ensure the stability of its textural and structural properties during reaction.

3. Loss of chemically bound water: The chemically bound water is removed at higher temperature.

4. Changes in pore size distribution and surface area due to sintering: Exposing the sample to high temperature over an extended period of time leads to some sintering and consequently decrease in surface area. Change in phase distribution: Higher temperature cause material to crystallize into different structural forms. Fig. 1 shows the formation of various phases of alumina when calcined at different temperatures.

3.3.1 Co Precipitation synthesis of undoped ZnO nanoparticles

Undoped ZnO nanoparticles are synthesized by co-precipitation method using $ZnSO_4.7H_2O$ as the starting material. The stoichiometric equation for the given synthesis is as follows:

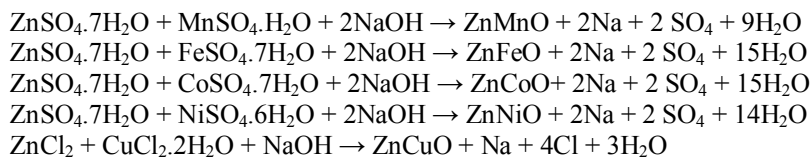$$ZnCl_2 + 2\ NaOH \rightarrow ZnO + 2Na + 2Cl + H_2O$$
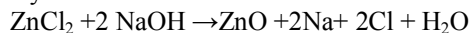
For this, a 0.2 M solution (sol A) of $ZnSO_4.7H_2O$ is prepared by dissolving 5.751 g of $ZnSO_4.7H_2O$ in 40 ml deionized water. This solution (sol B) is stirred for 1 hour. Another solution of 1M NaOH is prepared by dissolving 4g NaOH in 40 ml deionized water.

Sol B is then added to sol A. With the addition of NaOH, white precipitate is formed. This is due to the formation of hydroxide of zinc. Immediately 10 ml Ethylene Glycol (EG) is added, which acts as a capping agent, in order to control the size of the particles so formed. EG prevents the particles from agglomerating which leads to formation of larger sized particle. This solution is then aged for 15-16 hours while continuously stirring on a magnetic stirrer. After this, stirring is stopped and the precipitate is allowed to settle down. The precipitate is then washed repeatedly with water to remove all the alkaline impurity (unreacted NaOH). The filtered ppt. is then air dried at 150^0C for 5-6 hours. The resulting powder is then ground using mortal and pestel and further calcined at 450^0C for 5 hours. This gives nanoparticles of ZnO.

3.3.2. Co Precipitation Synthesis of Mn/Fe/Co/Ni/Cu doped ZnO:

For the synthesis of transition metal doped ZnO, $ZnSO_4.7H_2O$ and the sulphate salts of the respective metals are used. The calculations for the amount of precursors required are done as per the following stoichiometric equations:

$ZnSO_4.7H_2O + MnSO_4.H_2O + 2NaOH \rightarrow ZnMnO + 2Na + 2\ SO_4 + 9H_2O$
$ZnSO_4.7H_2O + FeSO_4.7H_2O + 2NaOH \rightarrow ZnFeO + 2Na + 2\ SO_4 + 15H_2O$
$ZnSO_4.7H_2O + CoSO_4.7H_2O + 2NaOH \rightarrow ZnCoO + 2Na + 2\ SO_4 + 15H_2O$
$ZnSO_4.7H_2O + NiSO_4.6H_2O + 2NaOH \rightarrow ZnNiO + 2Na + 2\ SO_4 + 14H_2O$
$ZnCl_2 + CuCl_2.2H_2O + NaOH \rightarrow ZnCuO + Na + 4Cl + 3H_2O$

According to the above stoichiometric equations, for the synthesis of 1 mol of doped ZnO, one mole of the precursors and 2 moles of the precipitating agent NaOH is required. The overall reaction is carried out in 100 ml solution. The molarity of zinc precursor and the doping metal precursors is taken to be 0.2 M while that of NaOH is taken to be 1 M. NaOH is taken in excess here so that no precursor is left unreacted.

For the synthesis, first of all, solutions of precursors are formed by dissolving the calculated amount in deionized water and stirring for 1 hour. The solutions of the precursors are mixed and then stirred again for 1 hour. After this, 1 M NaOH solution is added to the above mixture resulting in precipitation due to the formation of hydroxides of Zinc and dopant metals (Mn/Fe/Co/Ni). Immediately 10 ml Ethylene Glycol (EG) is added in order to control the size of the particles so formed. This solution is then aged by stirring for 15-16 hours. Later the precipitates are settled, filtered and washed repeatedly and kept for air drying at 150^0C for 4-5 hours. The powders so obtained are crushed and ground. These are then calcined at 500^0C for 4 hours in muffle furnace in order to obtain pure powders and eliminating undesirable compositions.

Characterization Techniques
4.1   X Ray Diffraction
X-ray diffraction (XRD) is an effective method for determining the crystal structure of materials. It detects crystalline materials having crystal domains greater than 3-5 nm. It is used to characterize bulk crystal structure and chemical phase composition.

Crystalline & Amorphous materials
Materials can be classified as:
Crystalline material: Crystalline material can be single crystal or polycrystalline
Amorphous material

Crystalline material
Crystalline materials are composed of atoms arranged in a regular ordered pattern in three dimensions. This periodic arrangement is known as crystal structure. It extends over distance much larger than the inter atomic separations. In single crystal this order extends through out the entire volume of the material. There are seven crystal system: cubic, tetragonal, orthorhombic, rhombohedral, hexagonal, monoclinic and triclinic. Different crystal structures are based on framework of one of the 14 Bravais lattice. Parallel planes of atoms intersecting the unit cell are used to define directions and distances in the crystal. The 'd spacing' is defined as the distance between adjacent planes. The orientation and interplanar spacing (d) of these lattice planes are defined by three integers h,k,l called Miller Indices. The (hkl) designate a crystal face or family planes throughout a crystal lattice.

Polycrystalline materials consist of many small single crystal regions called grains. Grains are separated by grain boundaries. The grains can have different shape and size and are disoriented with respect to each other.

Amorphous materials: When the atoms are not arranged in a regular periodic manner the material is called amorphous. Such material posses only short range order, distance less than a nanometer.

X-Ray Diffraction
X-ray is a form of electromagnetic radiation having range of wavelength from 0.01-0.7 nm which is comparable with the spacings between lattice planes in the crystal. Spacing between atoms in metals ranges from 0.2-0.3 nm. When an incident beam of X-rays interacts with the target atom, X-ray photons are scattered in different directions. Scattering is elastic when there is no change in energy between the incident photon and the scattered photon. In inelastic scattering the scattered photon loses energy.

These scattered waves may super impose and when the waves are in phase then the interference is constructive and if out of phase then destructive interference occurs.

Atoms in crystal planes form a periodic array of coherent scatterers. Diffraction from different planes of atoms produces a diffraction pattern, which contains information about the atomic arrangement within the crystal [1].

Bragg's law
The X-ray beams incident on a crystalline solid will be diffracted by the crystallographic planes. Bragg's law is a simple model explaining the conditions required for diffraction. It is given as n

$$\lambda = 2d_{hkl}\ \sin\theta$$
, where d_{hkl} is spacing between two planes hkl , n is an integer and λ is the wavelength. For parallel planes of atoms, with a spacing d_{hkl} between the planes, constructive interference occurs only when Bragg's law is satisfied. In diffractometers, the X-ray wavelength is fixed. Consequently, a family of planes produces a diffraction peak only at a specific angle θ.

The spacing between diffracting planes of the atoms determinses the peak positions. The peak intensity is determined by the atoms are in the diffracting plane. The Fig. 1 explains the Bragg's law. Two in-phase incident waves, beam 1 and beam 2, are deflected by two crystal planes (Z and Z_1). The diffracted waves will be in phase when the Bragg's Law, $n\lambda = 2d \sin \theta$, is satisfied. In order to keep these beams in phase, their path difference (SQ + QT) has to equal one or multiple X-ray wavelengths ($n\lambda$) i.e SQ + QT = $n\lambda$ or SQ + QT = $2PQ \sin \theta = 2d \sin \theta = n\lambda$. Hence the path difference depends on the incident angle (θ) and spacing between the parallel crystal planes (d).

4.2   Photoluminescence

Photoluminescence (PL) spectroscopy is a contactless, nondestructive method to probe the electronic structure of materials. Our capabilities include: various excitation wavelengths that allow for varying levels of volume excitation; a detection range extending from 0.4 to 2.7 μm; sample temperatures of 4 to 300 K; and mapping capabilities with 1- to 2-μm spatial resolution on the Fourier-transform-based system. The intensity and spectral content of the emitted photoluminescence is a direct measure of various important material properties, including:

Bandgap Determination. The spectral distribution of PL from a semiconductor can be analyzed to nondestructively determine the electronic bandgap. This provides a means to quantify the elemental composition of compound semiconductor and is a vitally important material parameter influencing solar cell device efficiency.

Impurity Levels and Defect Detection. The PL spectrum at low sample temperatures often reveals spectral peaks associated with impurities contained within the host material. The high sensitivity of this technique provides the potential to identify extremely low concentrations of intentional and unintentional impurities that can strongly affect material quality and device performance.

Recombination Mechanisms. The quantity of PL emitted from a material is directly related to the relative amount of radiative and nonradiative recombination rates. Nonradiative rates are typically associated with impurities and thus, this technique can qualitatively monitor changes in material quality as a function of growth and processing conditions.

4.3   Fourier Transform Infrared Spectroscopy (FTIR)

Fourier Transform Infrared Spectroscopy (FTIR) is a technique which is used to obtain an infrared spectrum of absorption or emission of a solid, liquid or gas. An FTIR spectrometer simultaneously collects high spectral resolution data over a wide spectral range [1].

FTIR offers quantitative and qualitative analysis for organic and inorganic samples. Fourier Transform Infrared Spectroscopy (FTIR) identifies chemical bonds in a molecule by producing an infrared absorption spectrum. The spectra produce a profile of the sample, a distinctive molecular fingerprint that can be used to screen and scan samples for many different components. FTIR is an effective analytical instrument for detecting functional groups and characterizing covalent bonding information. FTIR identifies chemical compounds in consumer products, paints, polymers, coatings, pharmaceuticals, foods, and other products [2].

The range of Infrared region is 12800 ~ 10 cm^{-1} and can be divided into near-infrared region (12800 4000 cm^{-1}), mid-infrared region (4000 ~ 200 cm^{-1}) and far-infrared region (50 ~ 1000 cm^{-1}). Infrared spectrum is molecular vibrational spectrum. When exposed to infrared radiation, sample molecules selectively absorb radiation of specific wavelengths which causes the change of dipole moment of sample molecules. Consequently, the vibrational energy levels of sample molecules transfer from ground state to excited state. The frequency of the absorption peak is determined by the vibrational energy gap. The number of absorption peaks is related to the number of vibrational freedom of the molecule. The intensity of absorption peaks is related to the change of dipole moment and the possibility of the transition of energy levels. Therefore, by analyzing the infrared spectrum, one can readily obtain abundant structure information of a molecule. The common used region for infrared absorption spectroscopy is 4000 ~ 400 cm^{-1} because the absorption radiation of

most organic compounds and inorganic ions is within this region [3]. The structural analysis of wurtzite ZnO was further supported through FTIR investigation, fig. 5.1.

Figure 8(a) corresponds to the wurtzite oxide stretching frequencies of ZnO. The main absorption bands at ~ 450 – 500 cm-1 (~ 4473x10-10 - 4970 x10-10 joule), which is the stretching mode of ZnO, was considered [4].

Results & Discussion
XRD Analysis:
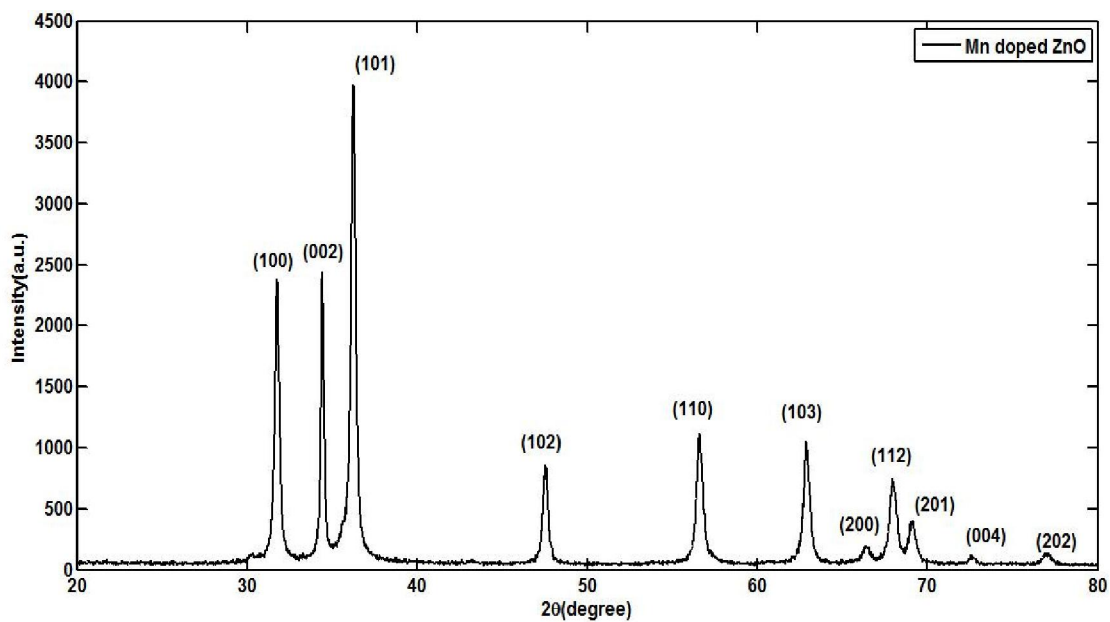
Mn doped ZnO:-

| Peak no.	2Θ	hkl	FWHM	d (A)	βCosθ	D (nm)
1.	31.7679	100	0.31	2.813	4.924	27.83
2.	34.4369	002	0.22	2.601	3.788	36.18
3.	36.2567	101	0.32	2.474	5.801	23.62
4.	47.5191	102	0.38	1.911	9.0286	15.18
5.	56.5978	110	0.45	1.624	12.735	10.76
6.	62.866	103	0.23	1.476	7.229	18.95
7.	66.4277	200	0.84	1.405	27.89	4.91
8.	67.9209	112	0.52	1.378	17.659	7.76
9.	69.1543	201	0.59	1.357	20.401	6.71
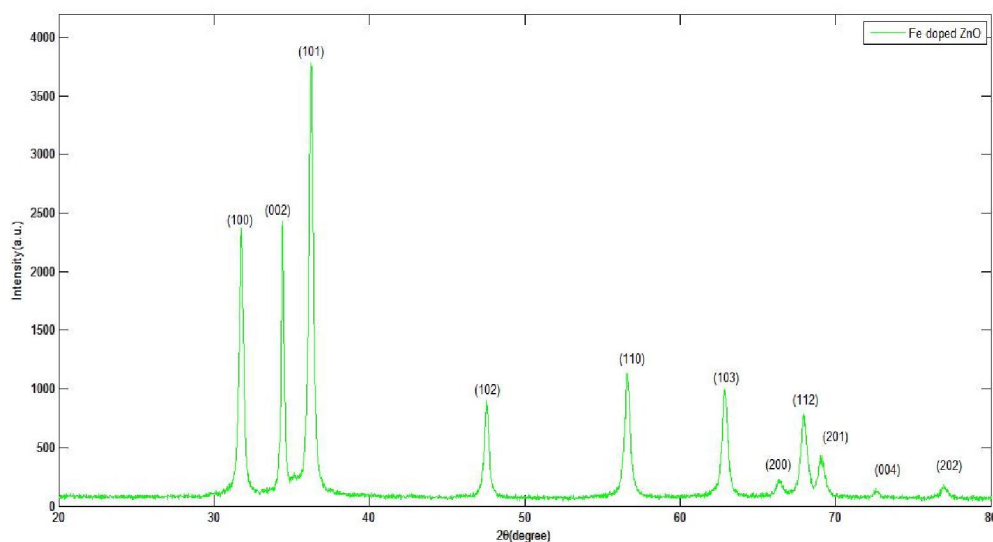
Fe doped ZnO:-

Peak no.	2Θ	hkl	FWHM	βCosθ	D (nm)
1.	31.7477	(100)	0.3375	5.6657	0.024191
2.	34.4167	(002)	0.2569	4.2831	0.032
3.	36.2567	(101)	0.4112	6.8204	0.020096
4.	47.5596	(102)	0.4112	6.5670	0.020871
5.	56.59	(110)	0.4112	6.3192	0.021689
6.	62.866	(103)	0.5140	7.6543	0.017906
7.	66.364	(200)	1.0280	15.016	0.009128
8.	67.9614	(112)	0.5140	7.437	0.018429
9.	69.0532	(201)	0.5140	7.3873	0.018429
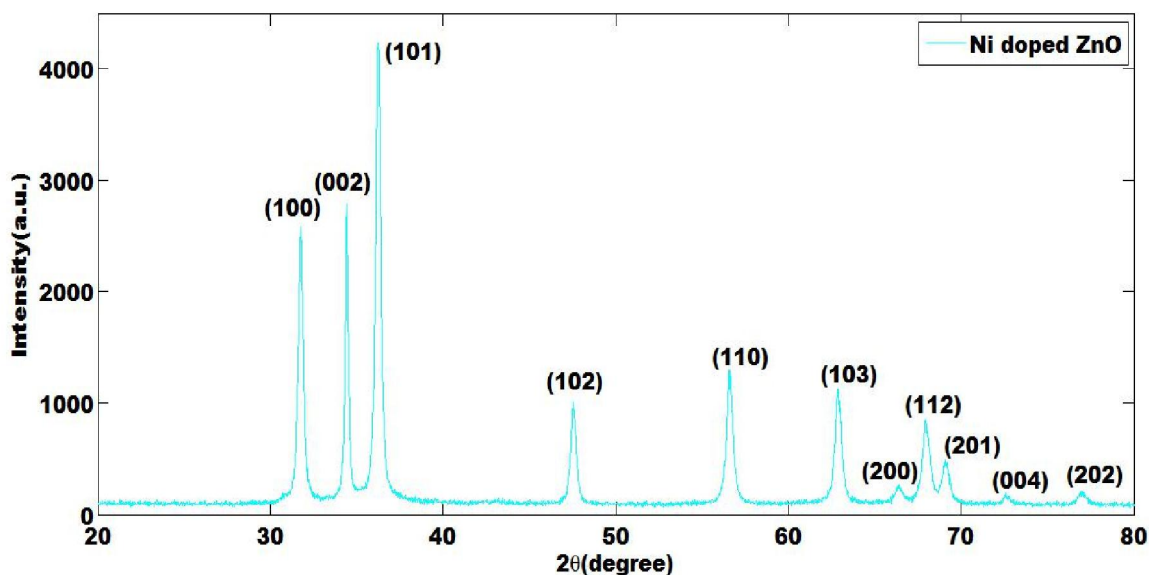
Ni doped ZnO:-

Peak no.	2Θ	hkl	FWHM	d (A)	βCosθ	D (nm)
1.	31.7679	(100)	0.34	2.813	5.401	23.90
2.	34.4167	(002)	0.22	2.602	3.442	36.09
3.	36.2365	(101)	0.34	2.476	6.160	24.18
4.	47.5394	(102)	0.38	1.910	9.032	24.90
5.	56.5978	(110)	0.44	1.624	12.452	21.90
6.	62.8862	(103)	0.46	1.476	14.464	19.14
7.	66.4247	(200)	0.93	1.405	30.887	11.94
8.	67.9614	(112)	0.56	1.378	19.029	17.88
9.	69.0937	(201)	0.65	1.358	22.455	14.68
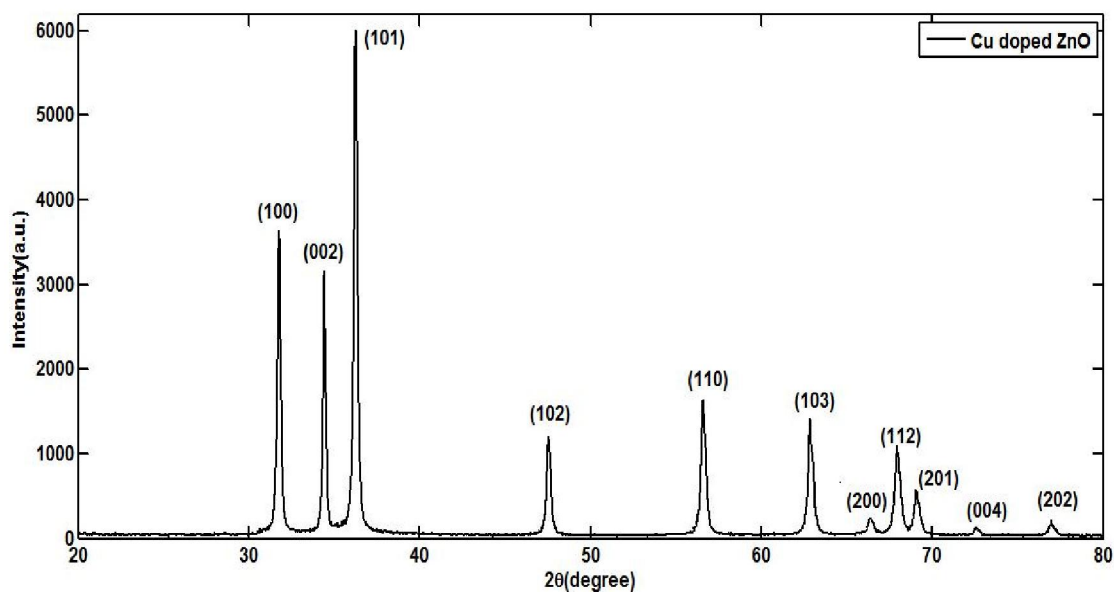
Cu doped ZnO:-

Peak no.	2Θ	hkl	FWHM	d (A)	βCosθ	D (nm)
1.	31.7477	(100)	0.23	2.82	3.651	35.84
2.	34.4167	(002)	0.2	2.602	3.442	41.26
3.	36.2567	(101)	0.24	2.474	4.351	35.82
4.	47.5191	(102)	0.28	1.911	6.653	30.13
5.	56.578	(110)	0.34	1.625	9.618	28.47
6.	62.866	(103)	0.35	1.476	11.002	26.94
7.	66.4044	(200)	0.44	1.406	14.608	21.26
8.	67.9411	(112)	0.38	1.378	12.908	28.18
9.	69.0532	(201)	0.39	1.358	13.465	25.36

Table 7.4 XRD Analysis of samples corresponding to Peak (101)

Sample	2θ (degree)	FWHM (β)	Grain Size (nm)	D values (Å)	Phase Assignment
ZnO	36.2365	0.3985	~21	2.4764	hexagonal
ZnO:Mn	36.2567	0.3211	~22	2.362	hexagonal
ZNO:Fe	36.24	0.4370	~19	2.4758	Hexagonal
ZnO:Co	36.28	0.4875	~17	2.4731	Hexagonal
ZnO:Ni	36.2365	0.3639	~24	2.418	Hexagonal
ZnO:Cu	36.2567	0.2339	~36	3.582	hexagonal

4.3.   FTIR Spectra:
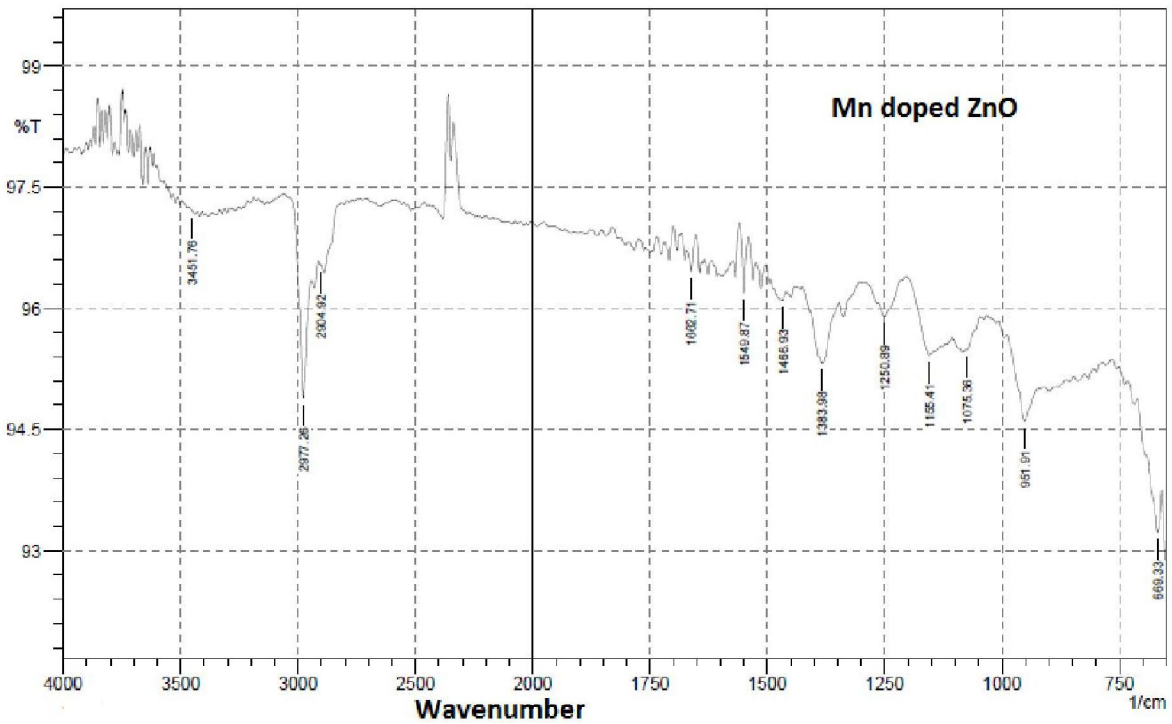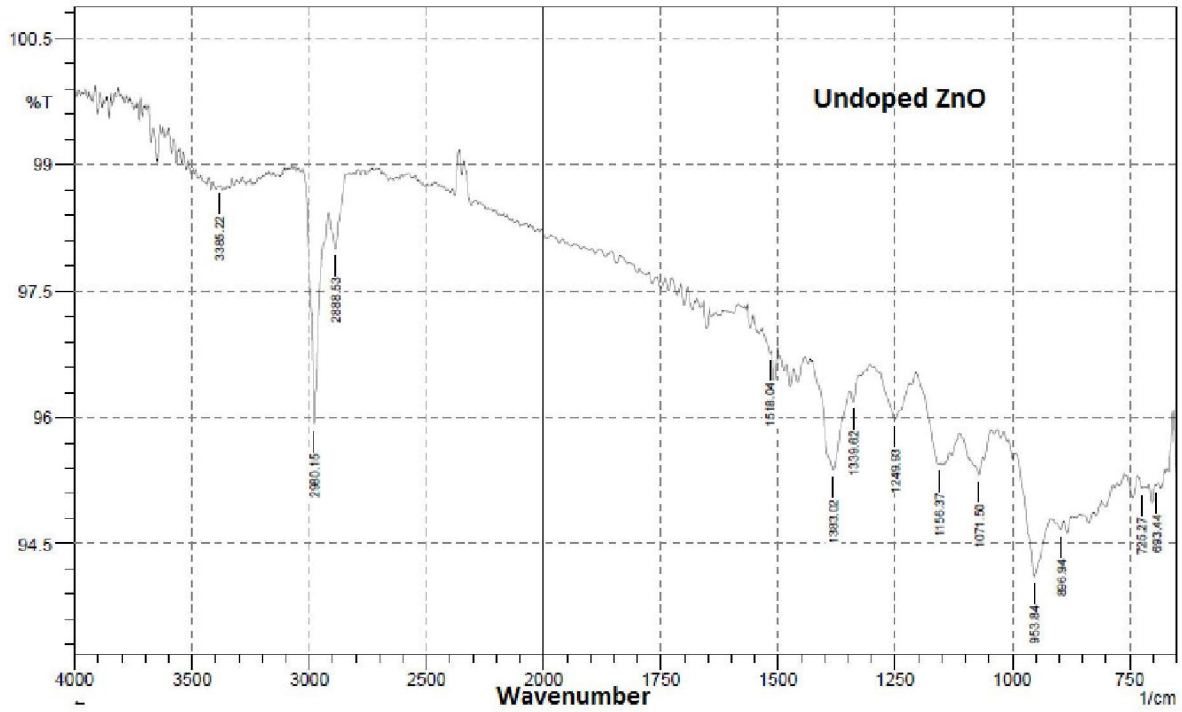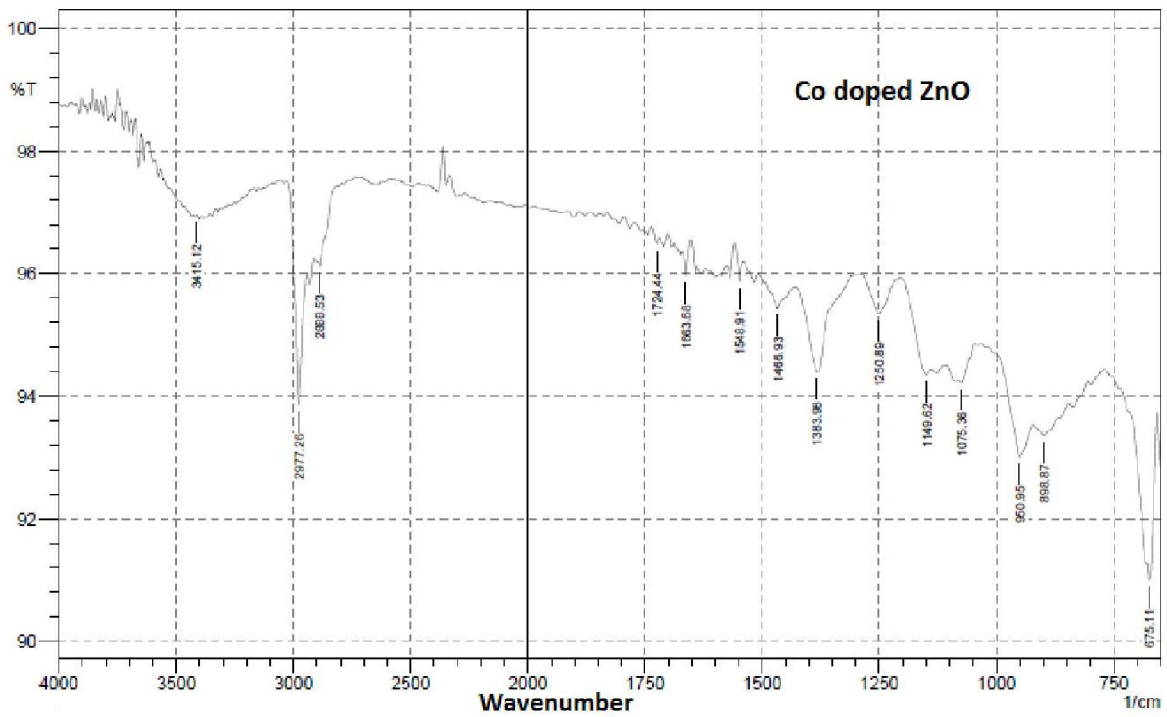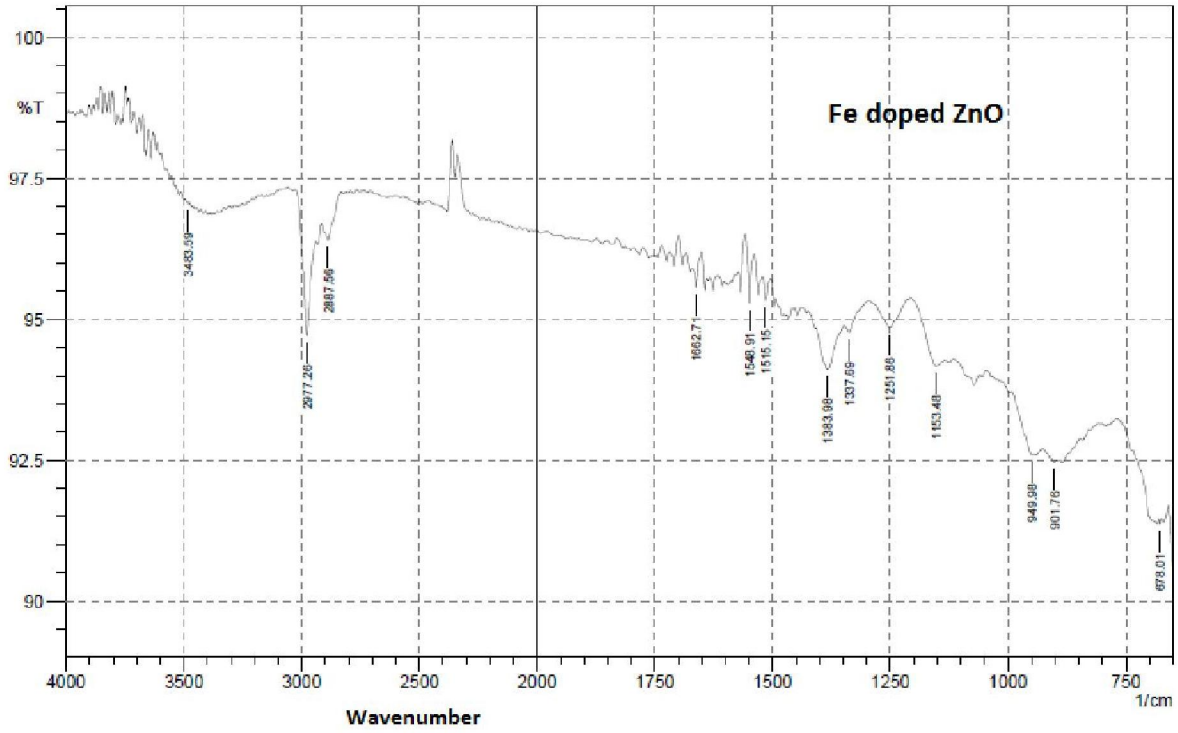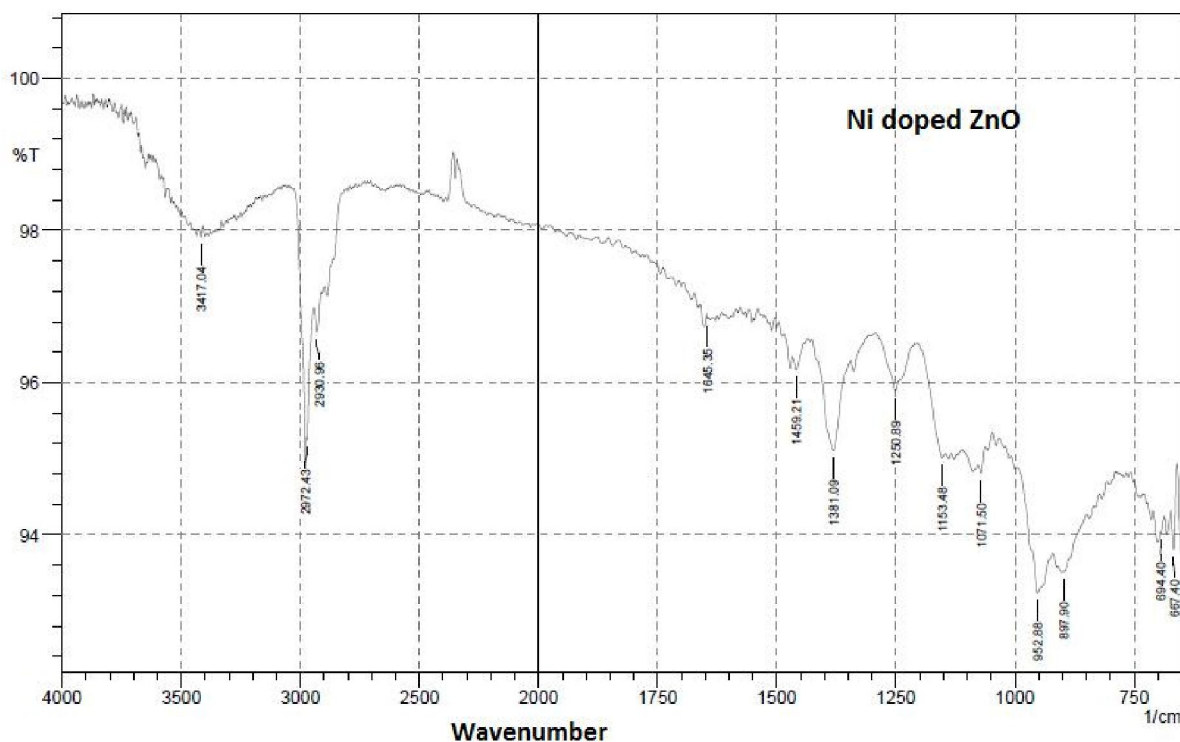
The FTIR spectra were recorded in the range of 650-4000 cm⁻¹ for all samples. The Zn-O bond is found around 420-450 cm⁻¹. The series of absorption in the current FTIR Spectra correspond to the impurities present in the samples. The peak at 667 cm⁻¹ is attributed to O=C=O bending vibration. This is due to the absorption of CO_2 from atmosphere due to preparation. The band in the region 670-1000 cm⁻¹ is due to =C-H bending of alkene while at 1660 cm⁻¹ is due C=C stretch of the same. The prominent peaks at 1071 cm⁻¹ and 1156 cm⁻¹ are because of C-O stretch (alcohol). The absorption bands observed around 1280 cm⁻¹ and 1330 cm⁻¹ correspond to C-O stretching (acid). The peaks around 1383 cm⁻¹ and 1460 cm⁻¹ reveal the presence of –C-H bending vibration of alkane and that around 2850-3000 cm⁻¹ reveal its C-H stretching vibrations. The broad absorption band in the region of 3400 cm⁻¹ corresponds to the O-H stretching vibrations of water present in the powder sample.

5.3　　　Photoluminescence

The photoluminescence originates from the recombination of surface states. The photoluminescence spectra over wavelength range 350-900 nm observed. The photoluminescence profile given in the fig. (7.8) deal with the emission spectrum of undoped ZnO, Ni doped ZnO and Cu doped ZnO with an excitation wavelength of 395 nm. PL spectra of undoped ZnO have highest intensity at the wavelength of 468.135nm which is corresponds to

blue emission of visible spectrum which is arises due to surface defects which may come during the grinding process of sintered sample and one other peak in red band. The spectrum exhibits two emission peaks, one is located at around (468.13 nm, 410.79nm and 411.79nm for undoped ZnO, ZnO:Ni and ZnO:Cu respectively) (UV region) corresponding to the near band gap excitonic emission [45] and the other is located at around 710 nm attributed to the presence of singly ionized oxygen vacancies [46]. The emission is caused by the radiative recombination of a photo generated hole with an electron occupying the oxygen vacancy [45]. Different level of bonding due to different materials (carrier) incorporation in the transition process is the main reason for different peaks. Generally oxide bond related peak shows in addition to main transition. We can calculate optical band gap of the material by using PL spectra. We have used formula-

$$Eg(eV) = \frac{h*c}{\lambda} \quad \text{............(6)}$$

Where h is the plank constant that is 6.6260×10^{-34} Joule, C is the speed of light 3×10^{10} m/sec and λ is the wavelength. By using this formula we found band gaps are 2.65eV, 3.02eV and 3.01eV of undoped ZnO, Ni doped ZnO and Cu doped ZnO respectively.
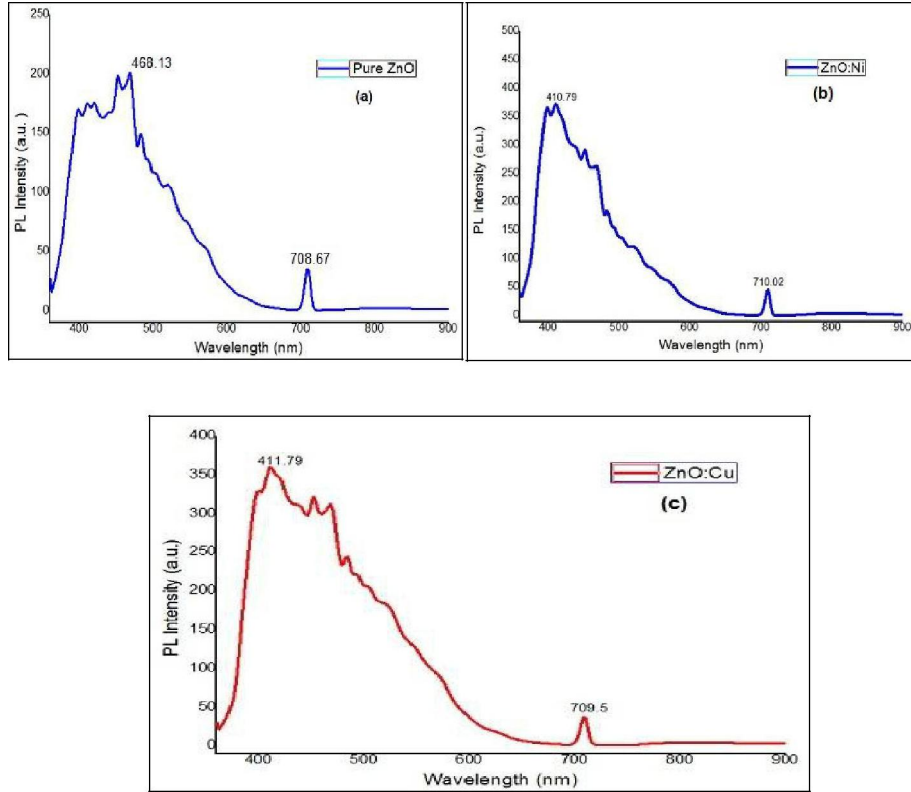
Figure 5.9 PL Pattern of (a) Undoped ZnO, (b)ZnO:Ni, (c)ZnO:Cu
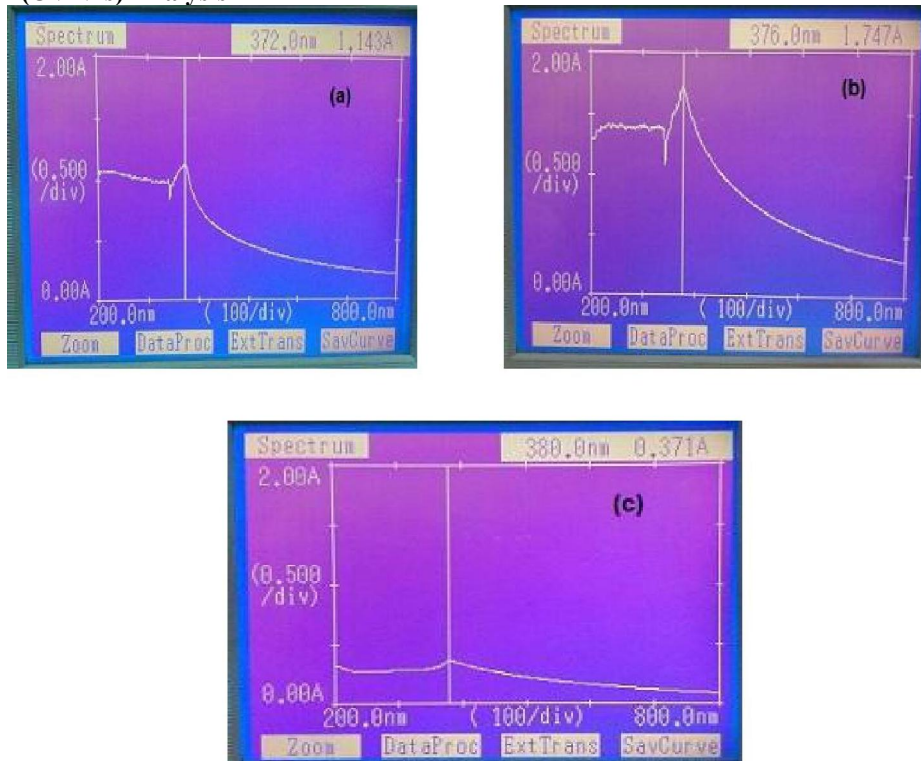
5.4 Absorption (UV-Vis) Analysis

Figure 5.11 UV-Vis Spectra of (a) ZnO, (b) ZnO:Ni, (c) ZnO:Cu

UV-Vis spectra are observed in the 200-800nm range. The prepared samples were first dispersed in water Before the UV Characterization we have dissolve 10mg of each sample in the 50ml DI separately to form a monodispersed solution. After this each sample was sonicated for 30 min. All three samples are not having any peak in the visible region. Optical absorption of Undoped, Nickel doped ZnO and Copper Doped ZnO are shown in fig. (5.11) the absorption spectra of undoped ZnO, ZnO:Ni and ZnO:Cu lie at 372nm, 376 and 380nm, respectively. The band gap values corresponding to these maxima are 3.33eV, 3.30eV and 3.26eV, respectively. These values are obviously red-shifted with respect to the band gap of undoped as well as bulk ZnO (3.37 eV).

6.1   Conclusion

We have successfully synthesized all three samples using simple co-precipitation method.

UV−Vis absorption spectra revealed red shift compared to the undoped ZnO, The structural analysis clearly indicate that pure phase of ZnO, ZnO:Ni and ZnO:Cu are formed and all have wurtzite structural. Pure ZnO sample has the lowest grain size that is ~20nm, Mn, Fe, Co, Ni doped and Cu doped ZnO have ~22nm and ~30nm respectively. Average strain is depends on the size of the particle as the size of the particle decrease strain is increases. PL spectra shows a blue shifting of peak wavelength from undoped ZnO to doped ZnO. Optical band gap is calculated using PL spectra and it was found 2.65eV, 3.02eV and 3.01eV of undoped ZnO, Ni doped ZnO and Cu doped ZnO respectively. Wavelength in UV-Vis spectra is shifted from lower to higher.

6.2   Future Work

1. Morphological study of prepared samples required (SEM, TEM).

2. Particle size analysis is required (DLS).

3. Raman Spectroscopy is needed for obtain space group.

4. Investigation of magnetic properties by using SQUID, VSM.

5. As a DMS in spintronics.

References 1:

1. Maity, R., A.N. Bannerjee and K.K. Chattopadhyay, Applied Surface Science, 236 (2004) pp. 231-235.
2. Maity, R., S. Das, M.K. Mitra and K.K. Chattopadhyay, Physica, E 25 (2005), pp. 605-612.
3. Maiti, U.N., P.K. Gosh, S. Nandy and K.K. Chattopadhyay, Physica, B 387 (2007), pp.103-108.
4. Li Y, Leung P, Yao L, Song QW, Newton E (2006) Antimicrobial effect of surgical masks coated with nanoparticles. J Hosp Infect 62:58-63.
5. Zhong Lin Wang, J. Physics: Condensed Matter 16 (2004) Zinc oxide nanostructures: growth, properties and applications.
6. Li Li Yang, Dissertation No. 1327, Synthesis and Characterization of ZnO nanostructures, Linkoping University, Sweden.
7. Rekha K, Nirmala M, Nair MG, Anukaliani A (2010) Structure, optical, photocatalytic, and anti bacterial activity of ZnO and Mn doped ZnO nanoparticles. Physica B 405:3180-3185.
8. X. Wang, Y. Ding, C.J. Summers, Z.L. Wang, J. Phys. Chem, B 108, 8773 (2004).
9. L.M. Kukreja, S. Barik, P. Misra, J.Cryst. Growth 268, 531 (2004).
10. J.W. Chiou, K.P. Krishna Kumar, J.C. Jan, H.M. Tsai, C.W. Bao, W.F. Pong, F.Z. Chien, M.-H. Tsai, I.-H. Hong, R. Klauser, J.F. Lee, J.J. Liu, and S.C. Liu, Appl. Phys. Lett. 85, 3220 (2004).
11. X.D. Bai, P.X. Gao, Z.L. Wang, E.G. Wang, Appl. Phys. Lett. 82, 4806 (2003).
12. P.Chang, Z. Fan, W. Tseng, D. Wang, W. Chiou, J. Hong, J.G. Lu, Chem. Mater. 16, 5133.
13. H. Chik, J. Liang, S.G. Cloutier, N. Kouklin, J.M. Xu, Appl. Phys. Lett. 84, 3376 (2004).
14. D. Banerjee, S.H. Jo, and Z.F. Ren, Adv. Mater. 16, 2028 (2004).
15. Y.-K. Tseng, C.-J. Huang, H.-M. Cheng, I.-N. Lin, K.-S. Liu, I.-C. Chen, Adv. Funct. Mater. 13, 811 (2003).
16. Y.W. Zhu, H.Z. Zhang, X.C. Sun, S.Q. Feng, J. Xu, Q. Zhao, B. Xiang, R.M. Wang, D.P. Yu, Appl. Phys. Lett. 83, 144 (2003).
17. Q. Wan, K. Yu, T.H. Wang, and C.L. Lin, Appl. Phys. Lett. 83, 2253 (2003).
18. Q.H.Li, Q. Wan, Y.J. Chen, T.H. Wang, H.B. Jia, and D.P. Yu, Appl. Phys. Lett. 85, 636 (2004).
19. P. Yang, H. Yan, S. Mao, R. Russo, J. Johnson, R. Saykally, N. Morris, J. Pham, R. He, H.-J. Choi, Adv. Mater. 12, 323 (2002).
20. W. I. Park, Y.H. Jun, S.W. Jung, and G. Yi, Appl. Phys. Lett. 82, 964 (2003).
21. Y. Gu, I.L. Kuskovsky, M. Yin, S.O'Brien, and G.G. Neumark, Appl. Phys. Lett. 85, 3833 (2004).
22. I. Shalish, H. Temkin, and V. Narayanmurti, Phys. Rev. B. 69, 245401 (2004).
23. Z. Fan, P. Chang, E.C. Walter, C. Lin, H.D. Lee, R.M. Penner. J.G. Lu, Appl. Phys. Lett. 85, 6128 (2004).
24. M. Joseph, H. Tabata, H. Saeki, K. Ueda, T. Kawai, Physica B 302-303, 140 (2001).

25. D.C. Look, D.C. Reynolds, C.W. Litton, R.L. Jones, D.B. Eason, G. Cantwell, Appl. Phys. Lett. 81, 1830 (2002).
26. K.-K. Kim, H.-S. Kim, D.-K. Hwang, J.-H. Lim, S.-J. Park, Appl. Phys. Lett. 83, 63 (2003).
27. J.C. Johnson, H. Yan, P. Yang, R.J. Saykalley, J. Phys. Chem. B 107, 8816 (2003).
28. www.geocities.jp/ohba_lab_ob_page/strucure6.html.
29. Z.L. Wang, X.Y. Kong, Y.Ding, P. Gao, W.L. Hughes, R. Yang, and Y. Zhang, Adv. Funct. Mater. 14, 943 (2014).
30. A.D. Corso, M. Posternak, R. Resta, and A. Balderschi, Phys. Rev. B 50, 10715 (1994).
31. M.H. Zhao, Z.L. Wang, and S.X. Mao, Nano Lett. 4, 587 (2004).

References 2:
1. Baruah S. Dutta J (2009) Hydrothermal growth of ZnO nanostructures, Sci Technol Adv Matter 10:01 3001 (18pp).
2. Liu B.Zeng HC (2004) Room temperature solution synthesis of monodispersed single crystalline ZnO nanorods and derived hierarchical nanostructures. Langmuir 20:4196-4204.
3. Xu F, Zhang P, Navrotsky A, Yuan ZT, RenTZ, Halasa M, Su B-L (2007) Hierarchially assembled porous ZnO nanoparticles: synthesis, suface energy and photocatalytic activity, Chem Mater 19:5680-5686.
4. Meulenkamp EA (1998) Synthesis and growth of ZnO nanoparticles. J Phys. Chem B 102:5566-5572.
5. www.wikipedia.com.
6. http://www.intertek.com/analysis/ftir/.
7. http://chemwiki.ucdavis.edu/Physical_Chemistry/Spectroscopy.
8. www.jnanobiotechnology.com/content/pdf/1477-3155-10-29.pdf.

12/25/2017